Supplementary Information (SI) for Chemical Science.
This journal is © The Royal Society of Chemistry 2026

Supplementary Information

cShot: Spatial Dynamic Imaging of Cell Cycle-Dependent miRNA Heterogeneity using Dynamic DNA Patterns

Jie Zhou, Yuwei Sha, Ling'ou Qin, Fengying Yuan, Yu Ouyang*, Yaqin Chai*, Pu Zhang*, Ruo Yuan*

Key Laboratory of Luminescence Analysis and Molecular Sensing (Southwest University), Ministry of Education, College of Chemistry and Chemical Engineering, Southwest University, Chongqing 400715, PR China

*Corresponding author. Tel.: +86-23-68252277; Fax: +86-23-68253172

Table of Contents

EXPERIMENTAL SECTION

Chemicals and Materials. All the DNA and RNA oligonucleotides were designed by customer and synthesized by Sangon Biological Engineering Technology & Co., Ltd (Shanghai, China) and purified using high-performance liquid chromatography. Lipo8000™ transfection reagent were purchased from Beyotime Biotechnology (Shanghai, China). Ethylenediaminetetraacetic acid (EDTA), Tris, $MgCl_2 \cdot 6H_2O$, HCl and boric acid were obtained from Sigma Chemical Co. (St. Louis, MO, U.S.A.). HEPES buffer were obtained from MedChemExpress (U.S.A.). TBE buffer solutions were composed of 59 mM Tris, 59 mM boric acid, and 2.0 mM EDTA, the pH was adjusted to 8.0. Deionized water was purified by a water purification system with a resistance of 18.2 MΩ·cm.

Table S1. Oligonucleotide sequences information used in the experiments

miRNA-21	UAG CUU AUC AGA CUG AUG UUG A
miRNA-196a	UAG GUA GUU UCA UGU UGU UGG G
miRNA-375	UUU GUU CGU UCG GCU CGC GUG A
miRNA-141	UAA CAC UGU CUG GUA AAG AUG G
ca	AGC TAC ATT GTC TGC TGG GTT TC
A	GAT ATC AGC GAT ACG ATA CTT AAC AC T CTG ATC AAT GCT AGC T
A'	TCAACATCAG GTGTTAAGTATCGT CACCCATGTTCGTCA
B	CTGCTCAGCGAT ACGATACTTAACAC CCCTCACTACCGAACCA
B'	GAA ACC CAG CAA AT GTG TTA AGT ATC GT CAC CCA TGT TAC TCT
A_{mod}	TTC TTC TTC TTC TTC TTC TTC GATATCAGCGAT ACG ATA CTT AAC AC TCTGATCAATGCTAGCT
B'_{mod}	GAA ACC CAG CAA AT GTG TTA AGT ATC GT CAC CCA TGT TAC TCTTTC TTC TTCT

H1	TCT CTG GCG ATC AGT ATT CGA CTA GT AGA GTA T rA GGA GCAG TCT AGT CGA ATA CTG ATC GCC ATTCG
H2	ACT AGT CGA AT-Cy5- A CTG ATC GCC AGA GAG ATG GCG ATC-BHQ2- AGT AT TCC TGA TCA
H3	TCT CTG GCG ATC AGT ATT CGA CTA GTT GAT CAG GAA TAC TGA TCG CC ATC
H_{1-2}	GGA GCAG TCT AGT CGA ATA CTG ATC GCC ATTCG
Sub1-noF(AB')	AGAGTA TrAGGA TATC
Sub2-noF(BB')	AGAGTA TrAGGAGCAG
Sub3-noF(BA')	TGACGA TrAGGAGCAG
Sub4-noF(AA')	TGACGA TrAGGA TA TC
Sub1	FAM-AGAGTA TrAGGA TATC-BHQ1
Sub2	ROX- AGAGTA TrAGGAGCAG-BHQ2
Sub3	CY5- TGACGA TrAGGAGCAG -BHQ2
Sub4	CY5.5-TGACGA TrAGGA TA TC-IBRQ
S1-A	ATT TAT CAC CCG CCA TAG TAG ACG TAT CAC CAG GCA GTT GAG ACG AAC ATT CCT AAG TCT GAA GAT ATC AGC GAT ACG ATA CTT AAC ACT CTG ATC AAT GCT AGCT
A'-S1	TCA ACA TCA GGT GTT AAG TAT CGT CAC CCA TGT TCG TCA ATT TAT CAC CCG CCA TAG TAG ACG TAT CAC CAG GCA GTT GAG ACG AAC ATT CCT AAG TCT GAA
B'-S1	GAA ACC CAG CAA ATG TGT TAA GTA TCG TCA CCC ATG TTA CTC TAT TTA TCA CCC GCC ATA GTA GAC GTA TCA CCA GGC AGT TGA GAC GAA CAT TCC TAA GTC TGAA
S1-B	ATT TAT CAC CCG CCA TAG TAG ACG TAT CAC CAG GCA GTT GAG ACG AAC ATT CCT AAG TCT GAA CTG CTC AGC GAT ACG ATA CTT AAC ACC CCT CAC TAC CGA ACCA
S1-random1	ATT TAT CAC CCG CCA TAG TAG ACG TAT CAC CAG GCA GTT GAG ACG AAC ATT CCT AAG TCT GAA TTA CGC ATT TTA CCG CGC AAA TTT CAA AAA TTT CGC AGA AAAT
Random2-S1	TTA TTA CGC ATT CGC AAC TTA TTA ATT CCG AAT AAT CGC_ATT TAT CAC CCG CCA TAG TAG ACG TAT CAC CAG GCA GTT GAG ACG AAC ATT CCT AAG TCT GAA

S2	ACA TGC GAG GGT CCA ATA CCG ACG ATT ACA GCT TGC TAC ACG ATT CAG ACT TAG GAA TGT TCG
S3	ACT ACT ATG GCG GGT GAT AAA ACG TGT AGC AAG CTG TAA TCG ACG GGA AGA GCA TGC CCA TCC
S4	ACG GTA TTG GAC CCT CGC ATG ACT CAA CTG CCT GGT GAT ACG AGG ATG GGC ATG CTC TTC CCG
Cy5-A	Cy5-GATATCAGCGAT ACG ATA CTT AAC AC TCTGATCAATGCTAGCT
Cy5-S2	Cy5-ACA TGC GAG GGT CCA ATA CCG ACG ATT ACA GCT TGC TAC ACG ATT CAG ACT TAG GAA TGT TCG
a1	AGAGTA TGGA TATC
a2	AGAGTA TGGAGCAG
a3	TGACGA TGGAGCAG
a4	TGACGA TGGA TA TC
MB probe	Cy5-AAG GTC AAC ATC AGT CTG ATA AGC TAC CTT-BHQ2
miRNA mimic	TAG CTT ATC AGA CTG ATG TTG A
miRNA inhibitor	T CAA CAT CAG TCT GAT AAG CTA

The ribonucleobase cleavage site, rA, in different substrates associated with Mg^{2+}-ion-dependent DNAzymes are indicated in red. The specific sequences of complementary base pairing are indicated in green.

Apparatus. The fluorescent response was detected by FL-7000 fluorescence spectrophotometer (Hitachi, Tokyo, Japan). pH-3C digital pH-meter (Shanghai LeiCi Device Works, Shanghai, China) was used to inspect the pH of all buffers during the experiment. Gel images were obtained by Gel Doc XR^+ System (Bio-Rad CA). Atomic Force Microscope (AFM) images were acquired by JPK NanoWizard 4 System (Bio-AFM GRE). Fluorescence imaging was operated on Olympus SpinSR10 spinning disk

confocal super resolution microscope (Olympus, Japan) with an objective lens (60 ×).

Simulated design of CDN reaction system in different states using NUPACK. The engineering design of the CDN reaction system was implemented through a multi-step computational and experimental workflow. Based on the principles of constitutional dynamic exchange, DNA sequences were optimized using the NUPACK software package to ensure structural stability, hybridization specificity, and catalytic functionality. As illustrated in the simulated hybridization schemes (Figure S3A), the rigid duplex stems of the four constituents were engineered with nearly identical thermodynamic stabilities (Gibbs free energy, $\triangle G$), thereby ensuring an unbiased dynamic exchange between different constituents. Consequently, NUPACK simulations predicted an equimolar distribution of the four constituents in the initial state.Structurally, each constituent integrates three functional domains: (i) a loop domain harboring an E6 DNAzyme for signal transduction via substrate cleavage; (ii) a tether domain designed for the recognition of DNA stimuli (T1 or T2); and (iii) a duplex framework for network reconfiguration. The dynamic transition is driven by a favorable thermodynamic gradient, where the hybridization of a trigger strand to the tether domain significantly lowers the system's free energy (from -22.92 to -42.94 kcal/mol). For instance, the introduction of T1 facilitates a constitutional reconfiguration from CDN "S" to CDN "X" by stabilizing constituent AA' while inducing the dissociation of AB' and BA'. Such stimulus-responsive population shifts and the resulting structural topographies were precisely predicted by NUPACK simulations (Figures S3B and S3C).

Preparation of CDNs. The [2×2] CDN "S", consisting of the components AA', AB', BA', and BB', was prepared as follows. A mixture of A, A', B, and B' (each at 4 μM) in HEPES buffer (10 mM, pH 7.2, 20 mM $MgCl_2$) was annealed at 65°C for 15 minutes. The solution was then cooled to 25°C at a rate of 0.33°C per minute, followed by equilibration at 25°C for 2 hours to yield the [2×2] CDN "S" comprising AA', AB', BA', and BB'. To induce transitions from CDN "S" to CDN "X" or CDN "Y", a 1 μM solution of CDN "S" (AA', AB', BA', BB') was mixed with the respective trigger, target miRNA-21 or competitive analogue (1 μM), and incubated at 37°C for 4 hours to obtain CDN "X" or CDN "Y", respectively.

Calibration curve of each constituent. 100 μL of the different concentration of each constituent: AA', AB', BA' and BB' was treated with their corresponding fluorophore/quencher-modified substrate. As an example, five samples of AA' at gradient concentrations (0.2 μM, 0.4 μM, 0.6 μM, 0.8 μM and 1μM) were prepared, and treated with the substrates: sub1 5 μL of 100 μM. Then establish a calibration curve based on the time-dependent fluorescence resulting from the catalytic activity of the Mg^{2+}ion-dependent DNAzyme.

AFM characterization of cShot. For the AFM experiment, 10 μL samples (100 nM) was dropped onto the smooth mica surface and leave to rest for 5 min, after that washed it with deionized water for 10 times and dried with nitrogen. The prepared sample was imaged on JPK NanoWizard 4 System (Bio-AFM GRE).

Cell Culture and Cell Lysate Preparation. The cell lines were purchased from the

American Type Culture Collection (ATCC) and cultured according to the provided protocols. MCF-7 cells (human breast adenocarcinoma cell line), MHCC97L cells (Human liver cancer cells) were selected as models for research. MCF-7 and MHCC97L cells were cultured in DMEM medium containing 1% non-essential amino acids, 100 U/mL penicillin and 10% fetal bovine serum (FBS) at 37 °C with a humidified atmosphere (95% air and 5% CO_2). After 24 h cultivation, 10^6 cells were collected in the exponential phase and washed twice with sterile PBS. The total RNA extraction for the real sample detection was obtained using the Trizol Reagent Kit (Sangon, Inc., Shanghai, China) according to the manufacturer's protocol. Finally, the obtained cellular extracts were diluted and stored at -20 °C for further use.

Cell cycle synchronizations. The cell cycle synchronization was achieved using serum deprivation to arrest cells at the G1 phase. Briefly, MCF-7 cells were cultured to the logarithmic phase and then switched to serum-free medium for 24 hours to induce cell cycle arrest due to the lack of growth factors. After synchronization, cells were re-stimulated by replacing the serum-free medium with fresh medium containing 10% fetal bovine serum (FBS), allowing the cells to progress through the cell cycle. For G1/S and S phase synchronization, a double-thymidine block method was used. First, cells were treated with 2.5 mM thymidine for 18 hours, followed by two washes with PBS and re-incubation in regular culture media. After 10 hours, a second thymidine block was applied by adding 2.5 mM thymidine for another 18 hours. Cells were collected at 24 hours (S) after release from the second block. To synchronize at G2/M and G1 phases, MCF-7 cells were seeded and grown to ~80% confluence. Cells were

then arrested with 50 ng/ml nocodazole in complete media for 16 hours. Following release into the cell cycle by the addition of regular media, cells were harvested at 0 hours (G2/M) and 7 hours (G1).

MiRNA-21 imaging in living cells using cShot.

Cells were plated on glass-bottom confocal dishes (MatTek P35G-1.5-14-C) at a density of 5×10^4 cells/cm² and cultured in complete DMEM medium (Gibco, 10% FBS) until 70% confluency. Prior to transfection, the medium was aspirated and replaced with serum-free Opti-MEM (Gibco). The cShot delivery was performed using a two-stage strategy: (1) Tetrahedral-stabilized CDNs (100 nM) were passively delivered into cells through membrane fusion at 37°C. (2) Following 2 h incubation (37°C, 5% CO_2), the secondary transfection complex was introduced using Lipo8000™: A mixture containing 200 nM H_1 hairpin and 800 nM each of H_2/H_3 hairpins in 100 μL serum-free medium was incubated with cells for 4 h. Post-transfection, cells were washed three times with PBS (pH 7.4, Gibco), maintained in phenol red-free imaging medium (Gibco 21063029), and immediately subjected to live-cell imaging using confocal microscope equipped with a 60× oil-immersion objective.

The kinetics simulation of CDN "S" converted to CDN "X" or CDN "Y".

Figure 2D showed time-dependent concentration changes of different constituents from CDN "S" to CDN "X", the specific concentrations of four constituents from the corresponding calibration curves are shown in the dots, and the simulation calculation

data is shown by solid line. The kinetic reactions associated with the time-dependent concentration changes of the constituents of CDN “X” upon subjecting the CDN “S” to the trigger strand T1 (miR-21) that shifts the equilibrium of the constituents in CDN “X” is summarized in equations (1) to (8). When CDN “S” is treated with trigger strand T1, the concentrations of AA' and BB' showed a robust increase in fluorescence after only 15 min of incubation at 37 ℃. And the concentration changes of the two constituents followed the first order reaction. The concentrations of AB' and BA' decreased accordingly.

Figure 2E showed time-dependent concentration changes of different constituents from CDN “S” to CDN “Y”, the specific concentrations of four constituents from the corresponding calibration curves are shown in the dots, and the simulation calculation data is shown by solid line. The kinetic reactions associated with the time-dependent concentration changes of the constituents of CDN “Y” upon subjecting the CDN “S” to the trigger strand T2 (ca) that shifts the equilibration of the constituents in CDN “Y” is summarized in equations (9) to (16). When CDN “S” is treated with trigger strand T2, the concentrations of AB' and BA' showed a robust increase in fluorescence after only 15 min of incubation at 37 ℃. And the concentration changes of the two constituents followed the first order reaction. The concentrations of AA' and BB' decreased accordingly. The experimental data points are obtained by time-dependent fluorescence at 25 °C for 30 min, the concentrations of the constituents are determined by the time-dependent fluorescence changes generated by the DNAzyme reporter units and using appropriate calibration curves in Figure S3.

Table S1. Rate constants of equations (1) ~ (8) (constituents exchanging reaction within the network) derived from the computational simulation of the transition of CDN "S" from CDN "X".

k_1	0.31644 $\mu M^{-1}min^{-1}$	k_2	12.38021 $\mu M^{-1}min^{-1}$
k_{-1}	0.27954 $\mu M^{-1}min^{-1}$	k_{-2}	0.79355 min^{-1}

Table S2. Rate constants of equations (9) ~ (16) (constituents exchanging reaction within the network) derived from the computational simulation of the transition of CDN "S" to CDN "Y".

k_1	0.31644 $\mu M^{-1}min^{-1}$	k_3	10.53227 $\mu M^{-1}min^{-1}$
k_{-1}	0.27954 $\mu M^{-1}min^{-1}$	k_{-3}	0.65471 min^{-1}

Supplemental Experiments

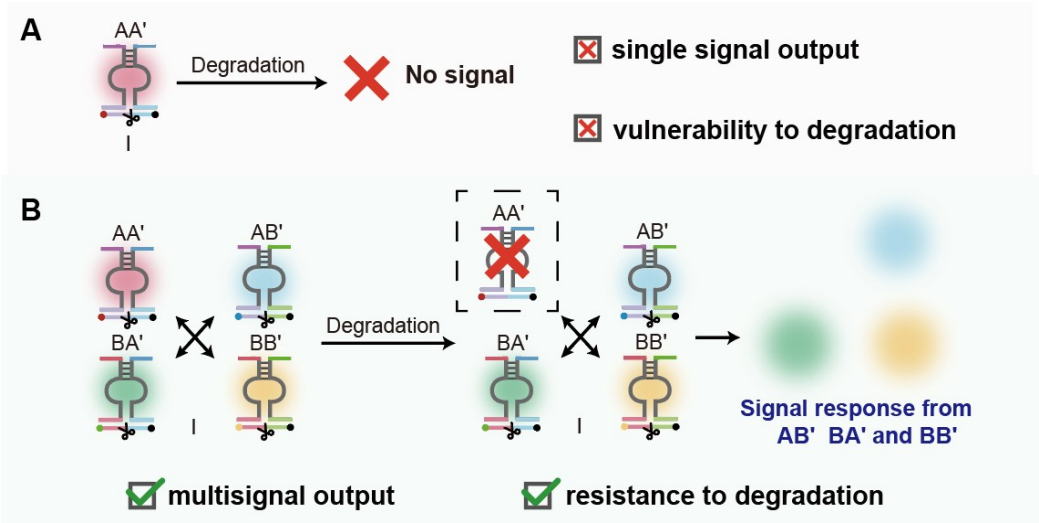

Figure S1. Traditional Switches vs. Constitutional Dynamic Networks. (A) Traditional switchable DNA conformations rely on single signal output derived from single sensing probe. (B) Constitutional dynamic networks (CDN) rely on the coordinated output of multiple signals.

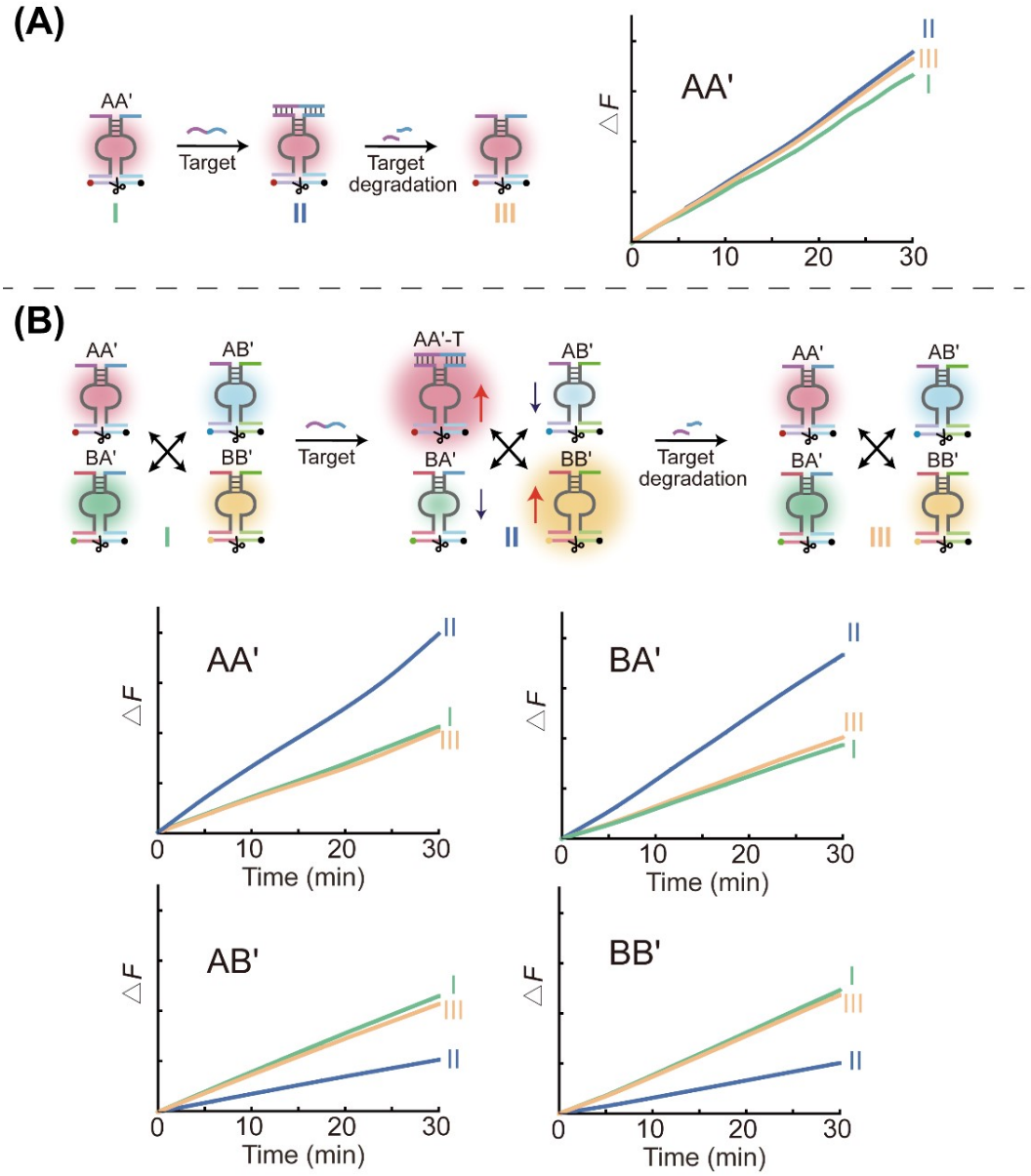

Figure S2. Kinetic Signal Output: Traditional *vs.* Dynamic DNA Systems. (A) Time-dependent fluorescence changes generated by DNAzyme reporter units associated with traditional target recognized molecules (AA'). (B) Time-dependent fluorescence changes generated by DNAzyme reporter units associated with constitutional dynamic DNA patterns.

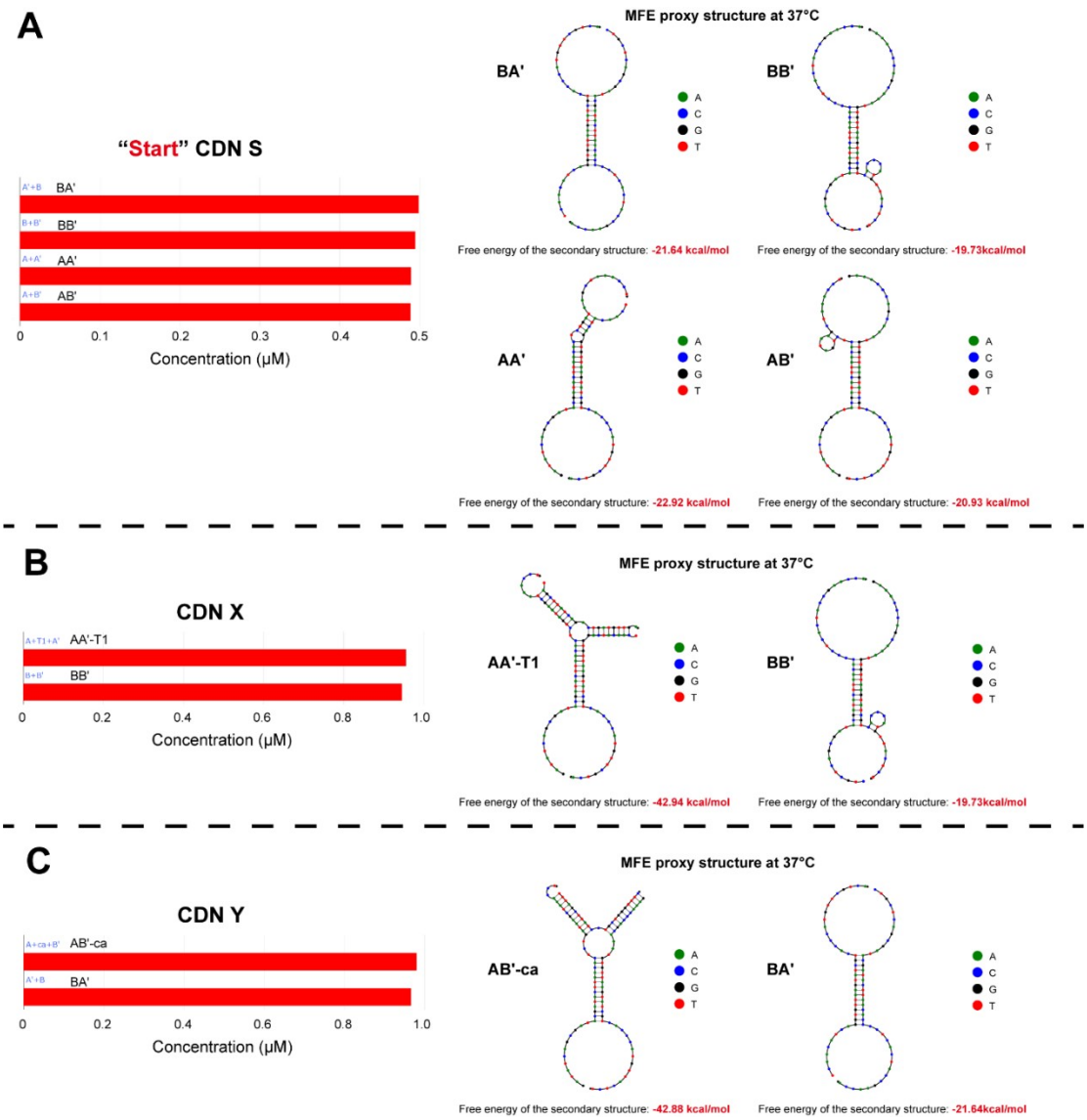

Figure. S3. Computational Modeling of CDN Assembly and Trigger-Driven Structural Reconfiguration. (A) The simulated hybridizing scheme of each constituent in CDN and the corresponding populations in CDN "S" presented by NUPACK software. (B) The structures of the constituents after subjection of T1 and their populations predicted by NUPACK software. (C) The structures of the constituents after subjection of T2 and their populations predicted by NUPACK software. NUPACK software calculation URL: https://alpha.nupack.org.

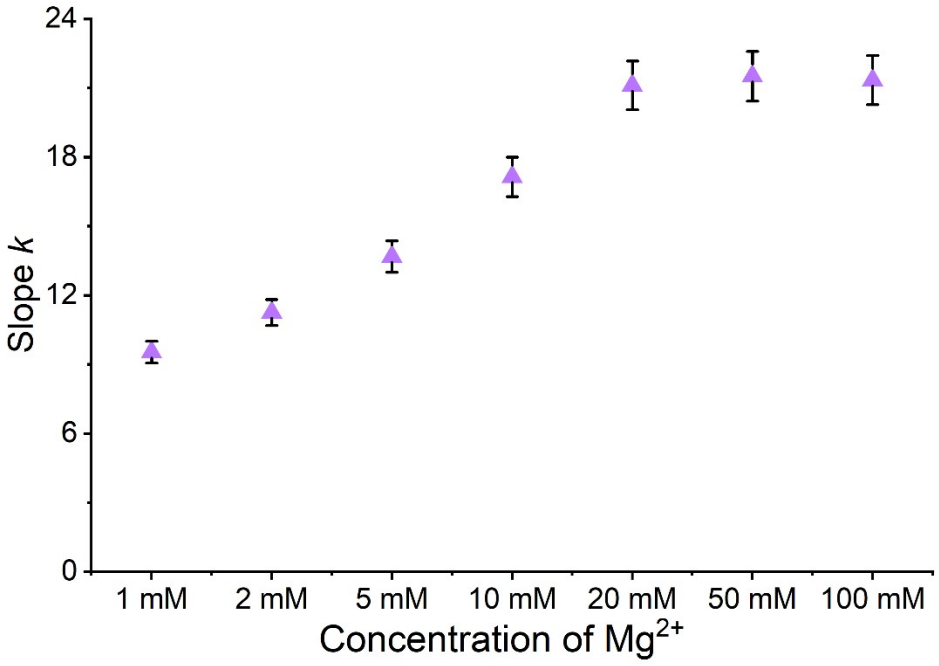

Figure S4. Optimization of Mg^{2+} concentration on the DNAzyme catalytic ability by adding the fluorophore/quencher substrates.

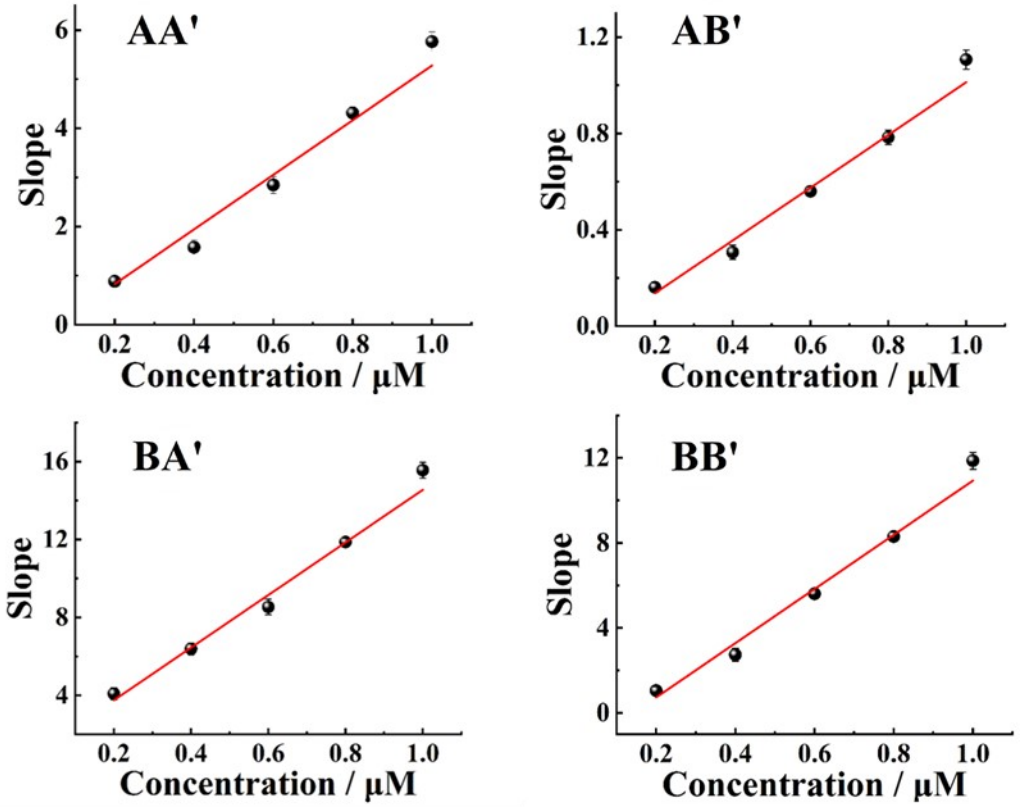

Figure S5. Calibration curves of CDN constituents. Calibration curves corresponding to the rates of the catalytic activities of the different constituents of the [2×2] CDN systems shown in Figure 3 as a function of their concentrations. Calibration curves are derived from the data shown in Figure 3B.

CDN	[BB']/(μM)	[AA']/(μM)	[AB']/(μM)	[BA']/(μM)
X	1.03	0.94	0.10	0.09
S	0.53	0.48	0.47	0.49
Y	0.05	0.05	0.91	0.96

Figure S6. Concentrations of the Constituents Associated with the Different CDNs.

Kinetic equations of the transsitions of CDN "S" to "X"

(1) $AA' + BB' \underset{k_{-1}}{\overset{k_1}{\rightleftharpoons}} AB' + BA'$

(2) $AA' + T_1 \underset{k_{-2}}{\overset{k_2}{\rightleftharpoons}} T_1AA'$

Derivatives:

(3) $\frac{d[AA']}{dt} = -k_1[AA'][BB'] + k_{-1}[AB'][BA'] - k_2[AA'][T_1] + k_{-2}[T_1AA']$

(4) $\frac{d[BB']}{dt} = -k_1[AA'][BB'] + k_{-1}[AB'][BA']$

(5) $\frac{d[AB']}{dt} = k_1[AA'][BB'] - k_{-1}[AB'][BA']$

(6) $\frac{d[BA']}{dt} = k_1[AA'][BB'] - k_{-1}[AB'][BA']$

(7) $\frac{d[T_1]}{dt} = -k_2[AA'][T_1] + k_{-2}[T_1AA']$

(8) $\frac{d[T_1AA']}{dt} = k_2[AA'][T_1] + k_{-2}[T_1AA']$

Figure S7. Computational simulation of the transitions of CDN "S" to CDN "X". The kinetic reactions associated with the time-dependent concentration changes during the transitions of CDN "S" to CDN "X" is summarized in equations (1) to (8). Knowing the time-dependent concentration changes of the CDNs constituents during the transitions of CDN "S" to CDN "X", we computationally simulated the time-dependent concentration changes of the constituents by using MATLAB R2022b.

Kinetic equations of the transsitions of CDN "S" to "Y"

(9) $AA' + BB' \underset{k_{-1}}{\overset{k_1}{\rightleftharpoons}} AB' + BA'$

(10) $AB' + T_2 \underset{k_{-3}}{\overset{k_3}{\rightleftharpoons}} T_2AB'$

Derivatives:

(11) $\frac{d[AA']}{dt} = -k_1[AA'][BB'] + k_{-1}[AB'][BA']$

(12) $\frac{d[BB']}{dt} = -k_1[AA'][BB'] + k_{-1}[AB'][BA']$

(13) $\frac{d[BA']}{dt} = k_1[AA'][BB'] - k_{-1}[AB'][BA']$

(14) $\frac{d[AB']}{dt} = k_1[AA'][BB'] - k_{-1}[AB'][BA'] - k_3[AB'][T_2] + k_3[T_2AB']$

(15) $\frac{d[T_2]}{dt} = -k_3[AB'][T_2] + k_{-3}[T_2AB']$

(16) $\frac{d[T_2AB']}{dt} = k_3[AB'][T_2] + k_{-3}[T_2AB']$

Figure S8. Computational simulation of the transitions of CDN "S" to CDN "Y". The kinetic reactions associated with the time-dependent concentration changes during the transitions of CDN "S" to CDN "Y" is summarized in equations (9) to (16). Knowing the time-dependent concentration changes of the CDNs constituents during the transitions of CDN "S" to CDN "X", we computationally simulated the time-dependent concentration changes of the constituents by using MATLAB R2022b.

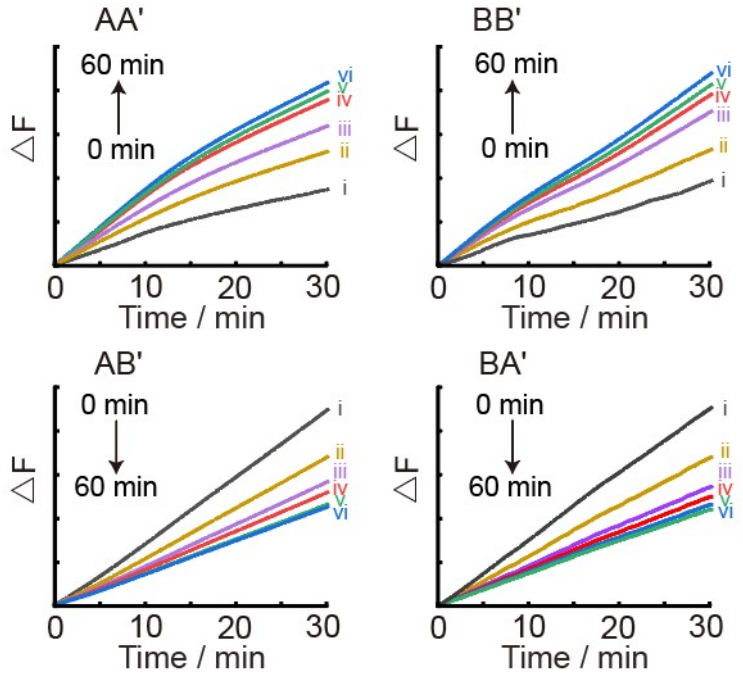

Figure S9. The kinetics simulation of CDN "S" converted to CDN "X". Time-dependent fluorescence changes generated by DNAzyme reporter units coupled to the constituents of CDN "X" upon subjecting the CDN "S" to the trigger T1, 1.0 μM. (i) 0 min, (ii) 5 min, (iii) 10 min, (iv) 15 min, (v) 30 min, (vi) 60 min.

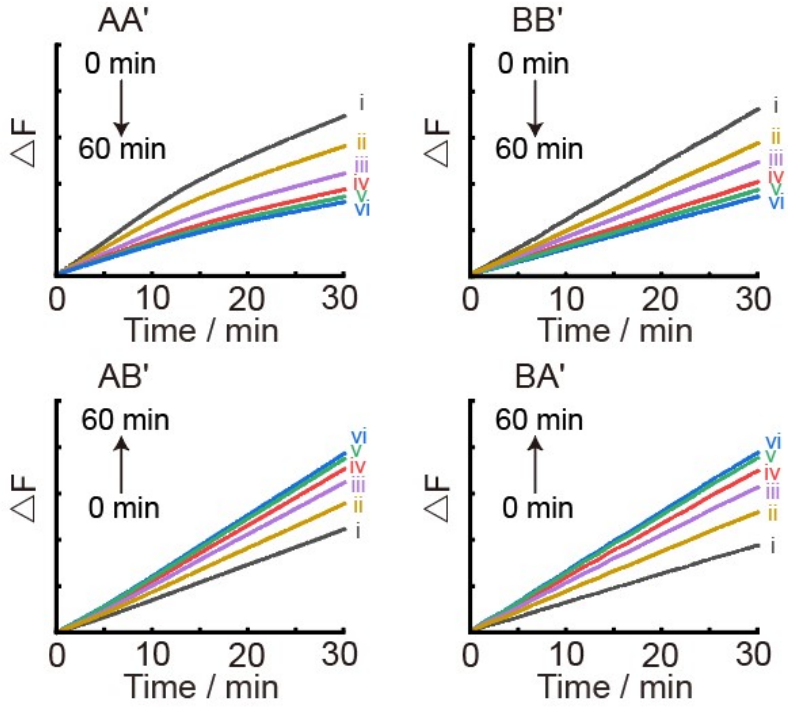

Figure S10. The kinetics simulation of CDN "S" converted to CDN "Y". Time-dependent fluorescence changes generated by DNAzyme reporter units coupled to the constituents of CDN "Y" upon subjecting the CDN "S" to the trigger T2, 1.0 μM. (i) 0 min, (ii) 5 min, (iii) 10 min, (iv) 15 min, (v) 30 min, (vi) 60 min.

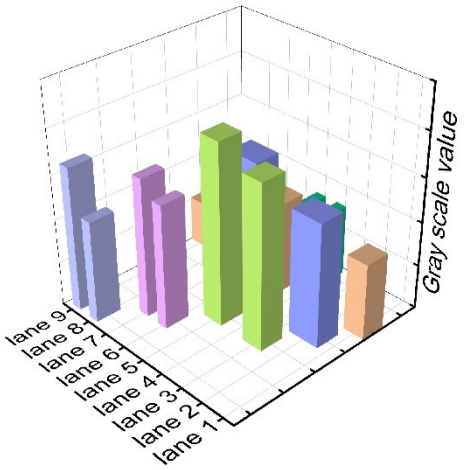

Figure S11. PAGE Characterization of the formation of CDN system and the conversion of CDN "S" to "X" or "Y". The quantitative gray scale value of Figure 2F. Lanes 1−4 correspond to the intact individual constituents, 1 μM each, BB', AA', AB', and BA'. Lane 5 is separated constituents of CDN "S". Lane 6 is reference intact constituent AA' stabilized by miR-21, AA'-T (1 μM). Lane 7 is separated constituents associated with CDN "X". Lane 8 is reference intact constituent AB' stabilized by competitive analogue, AB'-ca (1 μM). Lane 9 is separated constituents associated with CDN "Y".

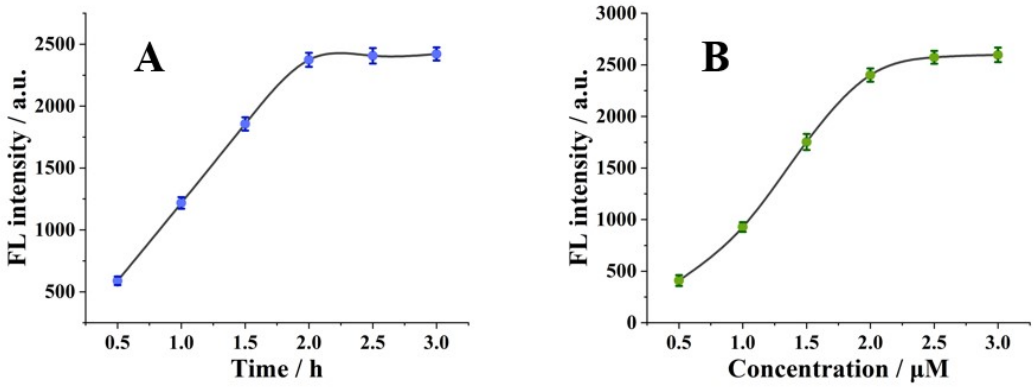

Figure S12. Optimization of HCR reaction conditions. (A) Relationship between the Cy5 fluorescence intensity and reaction time of HCR.; (B) Relationship between the concentration of H_2/H_3 and Cy5 florescence intensity.

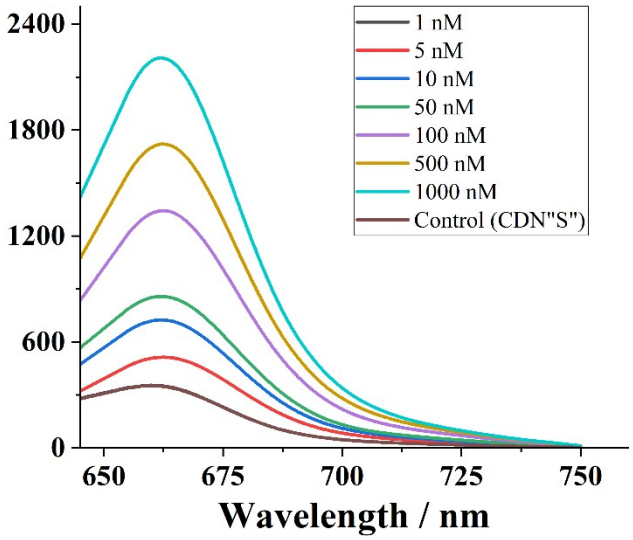

Figure S13. Calibration curves of target miR-21 by CDNs-guided HCR. Cy5 fluorescence signal induced by different concentration of target miR-21, control was the Cy5 fluorescence intensity(F0) generated by CDN "S" without miR-21.

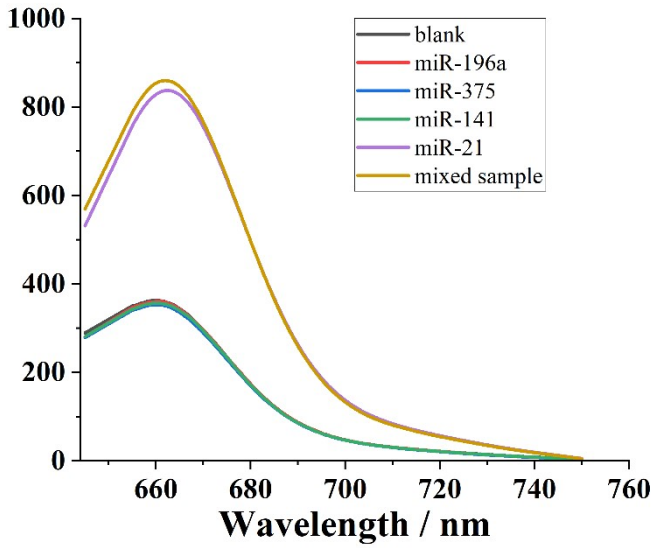

Figure S14. Specificity of the strategy based on CDNs coupled HCR system for miR-21. The concentration of target miRNA was 50 nM and the concentration of interfering miRNAs was 500 nM.

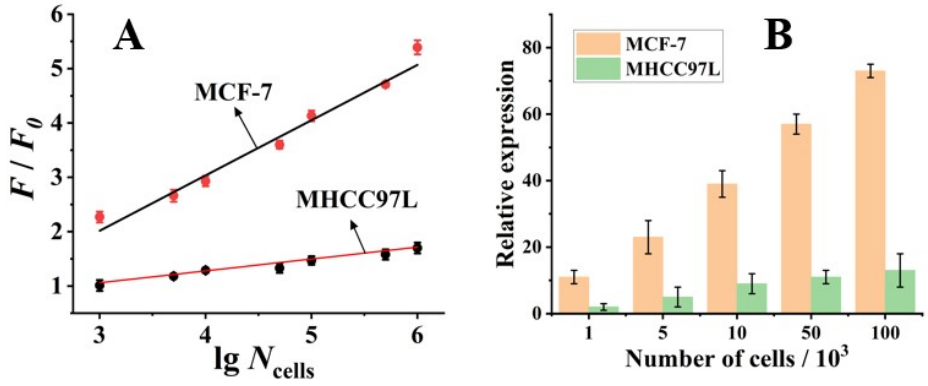

Figure S15. Calibration curve and miRNA-21 expression across different cell lines. (A) Calibration curve of the calculated Cy5 fluorescence intensity and the logarithm of cell numbers (1×10^3, 5×10^3, 1×10^4, 5×10^4, 1×10^5, 5×10^5, 1×10^6). (B) Relative expression of miRNA-21 in different cell lines determined by RT-qPCR (normalized to reference gene U6). Total RNA was extracted from MCF-7 cells and MHCC-97L cells.

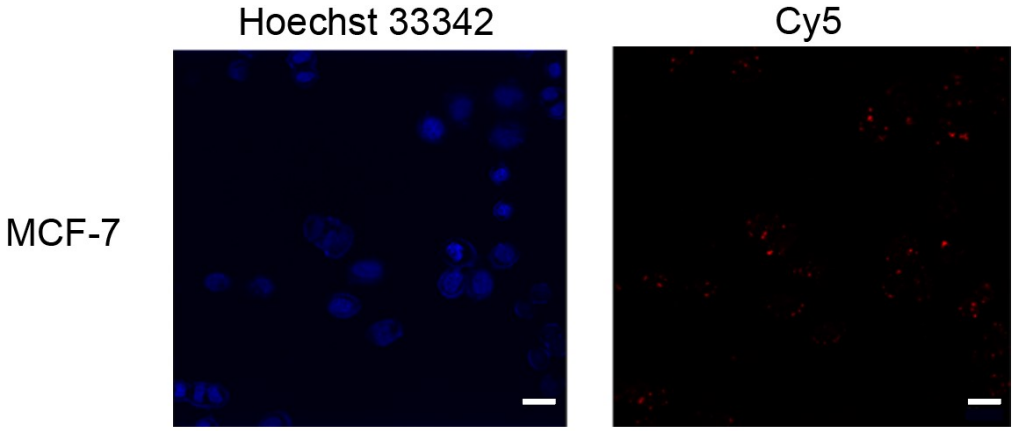

Figure S16. Confocal fluorescence images of MCF-7 cells treated with CDN-only system, H_1, H_2 and H_3. Scale bar: 20 μm.

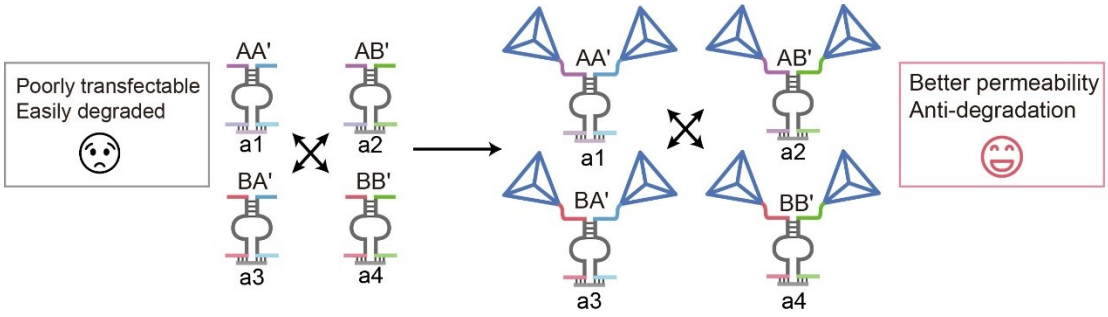

Figure S17. Schematic illustration of tetrahedra stabilized CDN system.

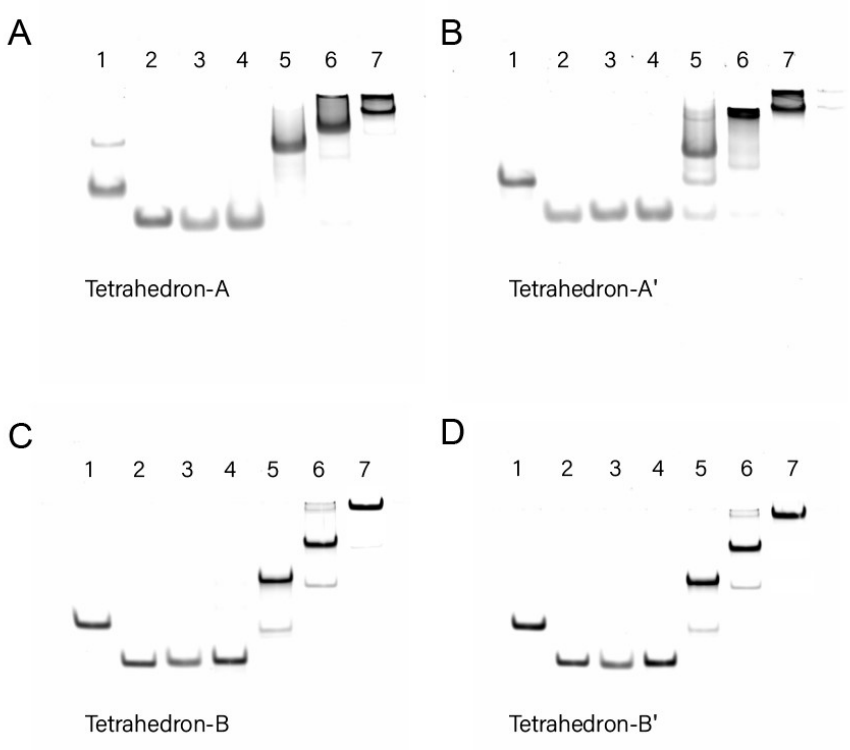

Figure S18. PAGE analysis of the tetrahedral stabilized CDNs presented in Figure S16. (A) lane 1-4 represented S1-A, S2, S3 and S4, lane5-7 represented S1-A+S2, S1-A+S2+S3, S1-A+S3+S3+S4. (B) lane 1-4 represented S1-A', S2, S3 and S4, lane5-7 represented S1-A'+S2, S1-A'+S2+S3, S1-A'+S3+S3+S4. (C) lane 1-4 represented S1-B, S2, S3 and S4, lane5-7 represented S1-B+S2, S1-B+S2+S3, S1-B+S3+S3+S4. (D) lane 1-4 represented S1-B', S2, S3 and S4, lane5-7 represented S1-B'+S2, S1-B'+S2+S3, S1-B'+S3+S3+S4. The final concentration for all the DNA in lanes is 1μM.

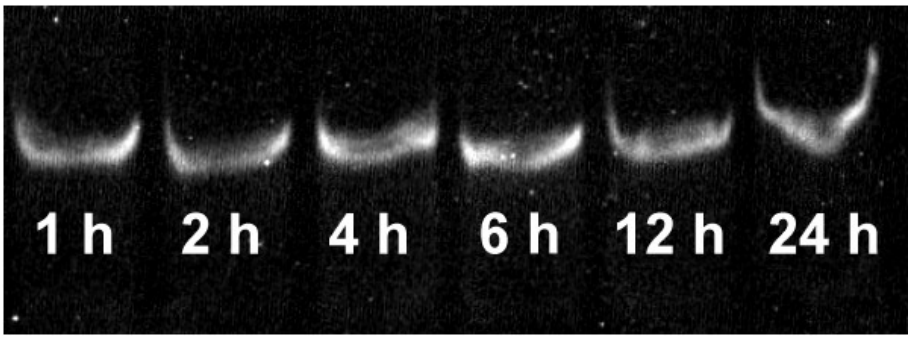

Figure S19. Investigation on the stability of the tetrahedral stabilized-AA' presented in Figure S17. the DNA probes (tetrahedron stabilized AA') were incubated in cell culture medium (supplemented with 10% FBS) at 37°C for various time intervals (1 h, 2h, 4 h, 6 h, 12 h, and 24 h).

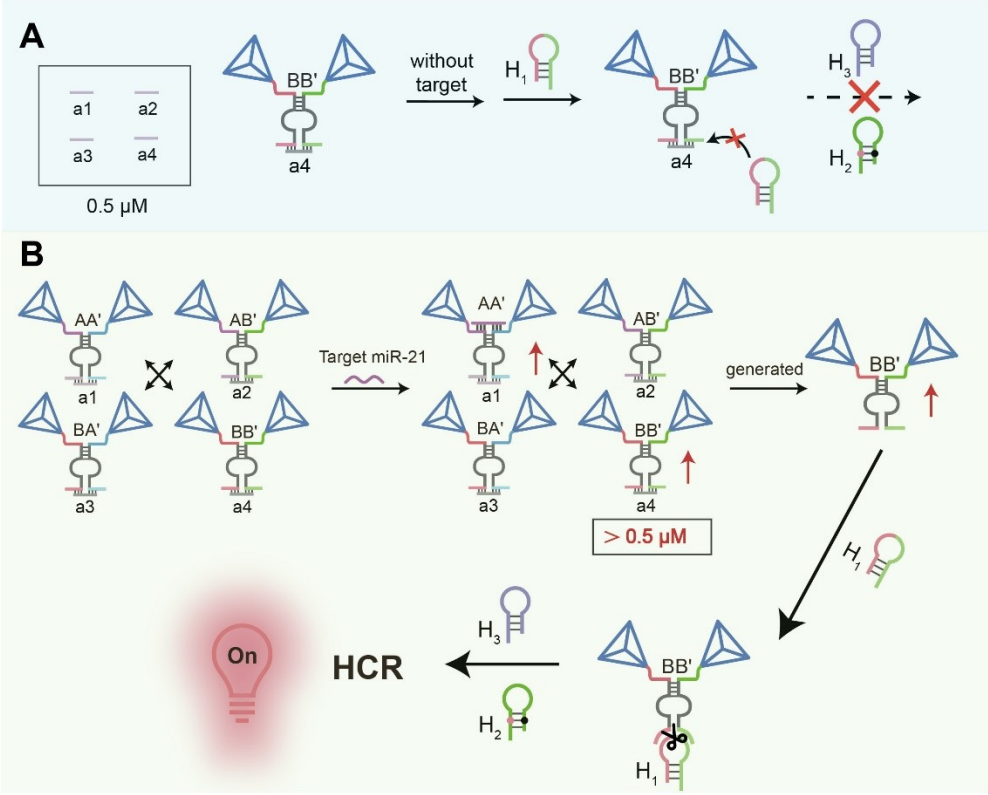

Figure S20. Schematic illustration of background suppression using four assistant strands. (A) In the absence of the target, assistant strands at equimolar concentrations with the CDN constituents effectively block the HCR reaction. (B) In the presence of the target miR-21, the concentration of BB′ exceeds that of the assistant strands, enabling successful initiation of the HCR process.

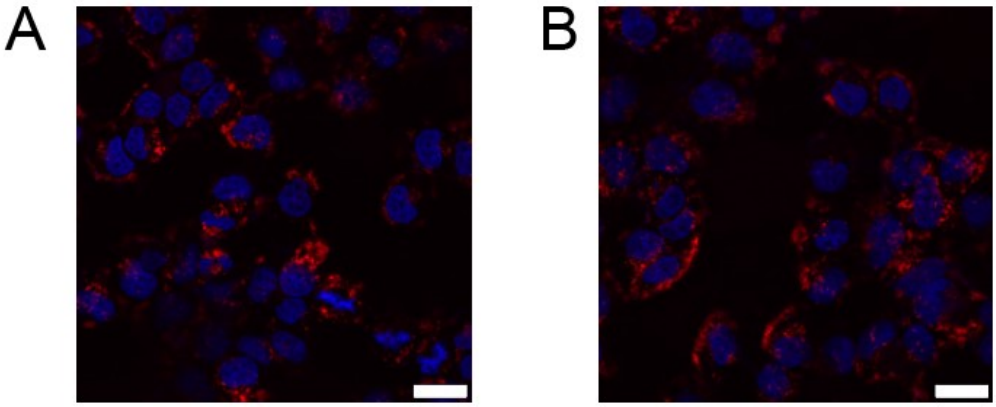

Figure S21. Intracellular miRNA imaging using tetrahedral-CDN system without assistant strands. (A) Confocal fluorescence images of MCF-7 cells. (B) Confocal fluorescence images of MHCC97L cells. Scale bar: 20 μm.

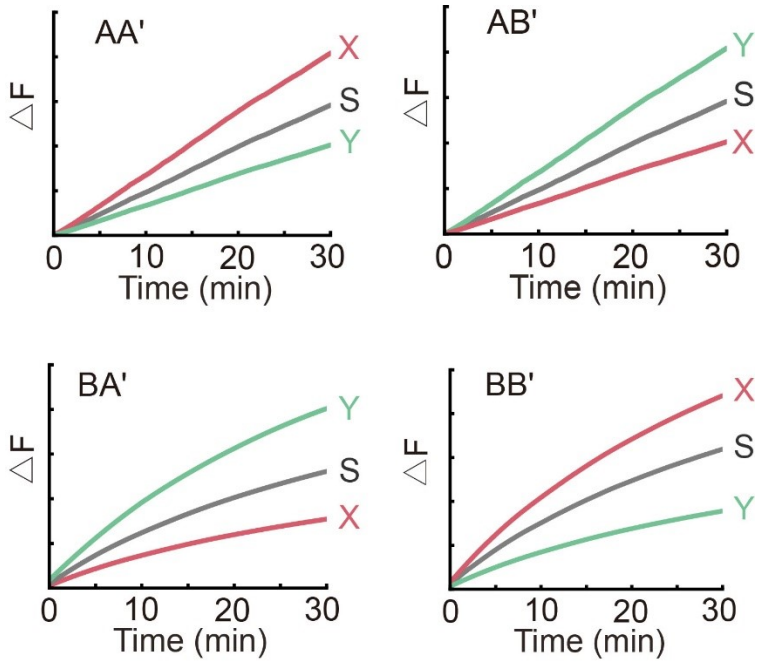

Figure S22. Time-dependent fluorescence changes of tetrahedra stabilized CDN system. Time-dependent fluorescence changes generated by the DNAzyme units associated with the different tetrahedra stabilized constituents, gray curve represented CDN "S", red curve represented CDN "X" after triggering CDN "S" with miR-21, green curve represented CDN "Y" after triggering CDN "S" with ca.

Comparative monitoring of intracellular miR-21 dynamics using a conventional molecular beacon (MB) and the cShot system.

Molecular beacons (MBs) are well-established, dual-labeled oligonucleotide probes that have been widely utilized for the sequence-specific detection of nucleic acids in living cells. As schematically illustrated in Figure S23A, The MB probe consists of a stem-loop structure, where a fluorophore and a quencher are brought into close proximity to maintain a "dark" state in the absence of a target. Upon hybridization with the target miRNA, the loop undergoes a conformational change that separates the fluorophore from the quencher, resulting in a “light up” fluorescence signal. In general, the comparative analysis between MB and cShot on miRNA visualization reveals that our platform offers significantly enhanced sensitivity through catalytic signal amplification and superior capability for real-time dynamic monitoring. First, under the identical imaging conditions and the concentration of DNA probes, the fluorescence intensity produced by MB functionalized with Cy5 and BHQ2 was significantly lower than that of the cShot system. This is attributed to the catalytic signal amplification, the embedded DNAzyme units and HCR strategy, inherent in our constitutional dynamic network, whereas MB relies on a 1:1 binding ratio of target. Secondly, while the MB showed minimal changes in fluorescence imaging of MCF-7 cells over time following NCS treatment, it failed to provide a distinct response rate to accurately reflect the dynamic fluctuations of miRNA levels (Figure S23B). The cShot system exhibited a robust and clear temporal variation in signal, reflecting its superior ability to track the dynamic flux of intracellular miRNA (Figure S23C). This

comparison underscores that traditional static MB probes are insufficient for capturing the complex dynamics of miRNA during physiological transitions, thereby justifying the necessity and advantage of our cShot platform. The corresponding normalized fluorescent intensity from Figure S23B and S23C are shown in Figure S23D.

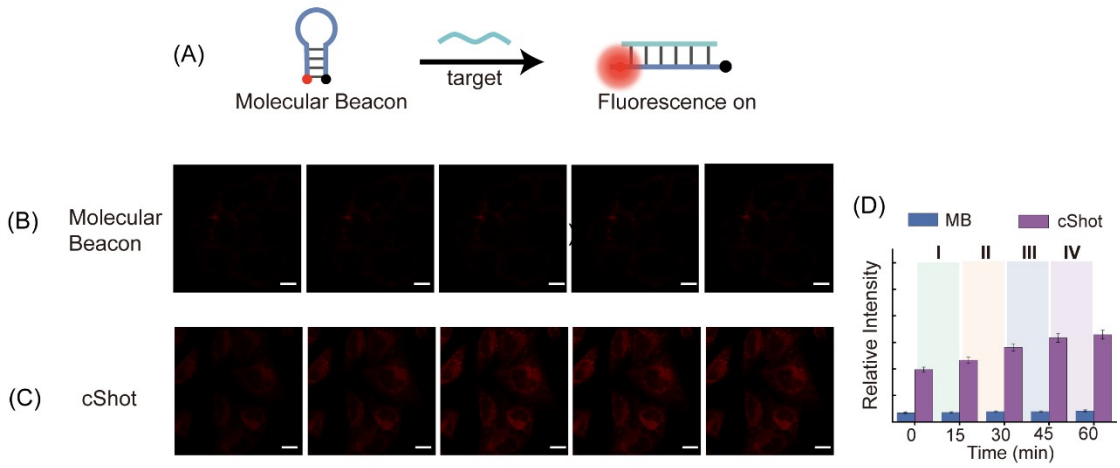

Figure S23. Comparative monitoring of intracellular miR-21 dynamics using a conventional molecular beacon (MB) and the cShot system. (A) Schematic illustration of the working principle of MB. (B) Confocal fluorescence images of NCS- treated MCF-7 cells using MB and (C) using cShot, respectively. Scale bar: 20 μm. (D) Quantitative analysis of the mean fluorescence intensity (MFI) derived from the images in (A) and (B).